

Accurate Calculations of the Peierls Stress in Small Periodic Cells

D.E. Segall

Department of Physics, Massachusetts Institute of Technology, Cambridge MA 02139

T.A. Arias

Laboratory of Atomic and Solid State Physics, Cornell University, Ithaca, NY 14853

Alejandro Strachan and William A. Goddard III

Materials and Process Simulation Center, Beckman Institute (139-74)

California Institute of Technology, Pasadena, Ca 91125

October 27, 2018

Abstract

The Peierls stress for a $[111]$ -screw dislocation in bcc Tantalum is calculated using an embedded atom potential. More importantly, a method is presented which allows accurate calculations of the Peierls stress in the smallest periodic cells. This method can be easily applied to *ab initio* calculations, where only the smallest unit cells capable of containing a dislocation can be conveniently used. The calculation specifically focuses on the case where the maximum resolved shear stress is along a $\{110\}$ -plane.

Key Words: Dislocation, Ab initio, Tantalum, Peierls stress, Boundary conditions

1 Introduction

Long, low-mobility $[111]$ -screw dislocations control low temperature plastic behavior in bcc metals. Unlike their fcc counter parts, bcc metals violate Schmid behavior and have many active slip planes. The microscopic origins of such behavior is crucial in the understanding of their plastic behavior. Therefore detailed and accurate first principle calculations are invaluable.

The Peierls stress, the zero temperature limit of the critical stress for slip, has been calculated in a variety of ways using various types of boundary conditions [1, 2, 3, 4, 5, 6, 7, 8]. These calculations, in general, rely on empirical potentials to simulate various configurations and incorporate a relatively large number of atoms. In general three types of boundary conditions are used, fixed cylindrical boundary conditions [2, 3, 4, 5], lattice greens functions [9, 6, 8] or periodic boundary conditions [1, 7]. For these approaches a large number of atoms is generally taken in order to minimize any artificial effects the boundary conditions may impose. Generally, this number is too large to be suited for *ab initio* calculations, even on the fastest and largest super-computers. Applying corrections to these effects is therefore important in order to have a reliable *ab initio* calculation.

The simplest approach is to use fixed cylindrical boundary conditions. However, care must be taken due to the mismatch of the boundary with the dislocation, particularly when the dislocation moves. This mismatch can be minimized by performing calculations in very large systems, effectively extrapolating to the limit of infinite cylinder size. The size of the system needed to extract accurate values can be greatly reduced by applying leading order corrections due to the mismatch in the boundary [2]. However, even with these corrections, accurate calculations can generally be

made only for a cylinder with a radius of $\sim 30\text{\AA}$ or greater, which corresponds to ~ 700 atoms when using periodic boundary conditions along the dislocation line. Such fixed cylindrical boundary conditions are generally ill-suited for an *ab initio* calculation due to both this large number of atoms and the artificial effects of the free surface at the boundary on the electrons. An alternative approach to account for boundary effects, and thereby reduce the size of the system needed for accurate calculation, is to use lattice greens function techniques [6, 8, 9]. This technique, although quite elegant, still faces the issue of free surface effects when applied to first principles quantum mechanical calculations.

Periodic boundary conditions are in general the most natural and straight forward way to calculate the Peierls stress in a density functional theory calculation. In periodic boundary conditions one is forced to have a net zero Burgers vector per unit cell. This is generally accomplished by using either a dipole or quadrupole array of dislocations [10, 11, 12]. Peierls stress calculations have been done in periodic boundary conditions using empirical potentials, however, to avoid dislocation-dislocation interactions, generally requires the use of unit cells [7] which would be impracticable for *ab initio* calculations. Wang *et al.*[1] have introduced a promising method for use in small, periodic cells, but this approach requires the decomposition of the total energy into individual atomic contributions, which while feasible for inter-atomic potential approaches, is not well-defined in quantum mechanical calculations.

In this paper it is shown how an accurate Peierls stress can be obtained in very small periodic cells. It is shown how leading order effects, due to the array of closely packed dislocations, can be accurately accounted. It is further shown how an accurate Peierls stress can be obtained by simply applying a pure shear to the system and minimizing the energy. This is a tremendous advantage in *ab initio* calculations as it minimizes the number of atomic configurations which need be explored. As an application of these ideas, we focus specifically on the calculation of the Peierls stress in bcc tantalum for a $[111]$ -screw dislocation in which the maximum resolved shear stress is along a $\{110\}$. This is among the most relevant geometries in understanding the plastic response of this material.

The paper is organized as follows. Section 2 presents the results of Peierls stress calculations in very large cylindrical cells, as a reference against which we shall compare our new approach. Section 3 presents the results of calculations using periodic boundary conditions and underscores the problems that arise. Section 4 shows how to overcome these problems, and, finally, Section 5 presents several techniques for accelerating the calculation. Finally, Section 6 concludes the paper.

2 Reference Calculations

All calculations presented throughout this manuscript employ a quantum-based, embedded atom force field (qEAMFF) developed in [13]. To provide the reference value of the Peierls stress for our calculations within periodic boundary conditions, we first perform calculations for isolated dislocations in a cylindrical geometry with fixed boundary conditions.

To form the dislocation, we proceed as follows. First, we define coordinates for our calculations as follows: the x -axis lies along the $[1\bar{1}0]$ direction, the y lies along the $[11\bar{2}]$, and the z lies along the $[111]$. A cylinder with radius $R2$ of Ta is then taken (Figure 1) which has two regions, a fixed region and a relaxation region. In the relaxation region ($r < R1$), where r is the radial distance from the center, the atoms are allowed to relax in response to their interatomic forces. The atoms in the fixed region ($R1 < r < R2$) are held fixed to their positions according to the solution of anisotropic elasticity theory. Finally, periodic boundary conditions (with period of one Burger's vector) are employed along the direction of the dislocation. Thus, these calculations consider only straight, infinite dislocations. A $[111]$ -screw dislocation then is obtained by displacing all atoms in

the cylinder according to the solution of anisotropic elasticity theory [14, 15] and then optimizing the positions of the atoms in the relaxation region.

To calculate the Peierls stress, we then apply a strain to the system which ensures that the resulting stress has only one component, σ_{xz} , which generates a force on the dislocation line in the $[11\bar{2}]$ direction [16]. We then optimize the locations of the atoms in the relaxation region subject to this external strain. Figure 2 shows the resulting dislocation structure in a large cylinder ($R1 \approx 120\text{\AA}$) for a series of different strains using a differential displacement (DD) map [17]. In these maps, the circles represent columns of atoms viewed along the $[111]$ direction. The arrows indicate the change in relative displacement that neighboring atomic columns make, relative to the bulk, due to the presence of the dislocation. The lengths of the arrows are normalized so that a displacement of $1/3$ of a Burgers vector corresponds to an arrow of full length. The first panel (a) shows the ground-state structure of the dislocation at zero stress. The center of the dislocation is located at a diamond encased in triad of arrows. Going around this triad makes three displacements of one-third of a Burgers vector for a net displacement of one full Burgers vector relative to the bulk. The ground state structure of the core is seen to break the symmetry of the lattice by extending outward along three $\{110\}$ planes. This “degenerate split core” is consistent with molecular dynamic results, using periodic boundary conditions, found in reference [1] when using the same interatomic potential.

As the strain is applied to the ground state structure (Figures 2b-d), the dislocation feels force along the $(1\bar{1}0)$ -plane. As the applied strain obtains a critical value, the dislocation center moves one lattice spacing along the $(1\bar{1}0)$ -plane (Figure 2b). As the strain is increased further, the dislocation then glides along the $(2\bar{1}\bar{1})$ (Figures 2 c,d) in two steps, first along $(10\bar{1})$ and then spontaneously along $(1\bar{1}0)$. There are consequentially two Peierls barriers that the dislocation must overcome, the first along $(1\bar{1}0)$ and the second along $(10\bar{1})$. This leaves some ambiguity for the definition of the Peierls stress. Different authors have used different definitions [1, 4, 5, 6]. For clarity we will consider the value of the σ_{xz} stress for the first jump (Figure 2a-b) as the first Peierls stress ($P1$) and the value of the σ_{xz} stress for the second jump (Figure 2b-c) as the second Peierls stress ($P2$).

To extract the limit of these critical stresses for an isolated dislocation in an infinite crystal, we have repeated the above calculations in cylinders of various sizes ranging from $R1 = 30\text{\AA}$ to $R1 = 120\text{\AA}$ and extracted the Peierls stress as a function of radius. Figure 3 summarizes our results. In the limit, we find values of 0.74 GPa and 0.91 GPa for $P1$ and $P2$, respectively.

As a consistency check that we indeed expect finite-size effects to be small for our largest cylinders, one can employ the method of Shenoy and Phillips [2]. This method estimates the unaccounted restoring stress that the boundary applies to a displaced dislocation to be

$$\frac{K_s b}{2\pi} A \frac{d}{R^2},$$

where $K_s = (S_{11}/(S_{11}S_{44} - S_{15}^2))^{1/2}$ in terms of the modified elastic compliances S_{ij} [14], b is the Burgers vector, d is the distance the dislocation has moved from the center of the cylinder, R is the radius of the cylinder, and A is a dimensionless constant that can be calculated through elasticity theory or computationally. In our case, $A \approx 2$, $K_s = 68\text{GPa}$ and $b = 2.9\text{\AA}$. Finally, for $P1$ we have $d \approx .1\text{\AA}$ and for $P2$ we have $d \approx 2.7\text{\AA}$. For our largest cylinder ($R1 = 120\text{\AA}$), we calculate a restoring stress of 0.0004GPa and 0.012GPa, respectively. Both values are quite small, well within the uncertainties in Figure 3.

3 Periodic Boundary Conditions

In periodic boundary conditions, the unit cell must contain a net zero Burgers vector. In practice this is generally accomplished through the use of either a dipolar or quadrupolar array of dislocations [10, 11, 12]. Our calculations employ a quadrupole array, which has been shown to be the more appropriate choice for screw-dislocations [12]. Figure 4 illustrates a cell containing 270 atoms.

As our first attempt to calculate the Peierls stress in periodic boundary conditions, we take a quadrupole array with lattice vectors fixed at the values corresponding to the perfect bulk material, that is the appropriate lattice vectors prior the insertion of dislocations. Below, we refer to this choice as “unrelaxed” lattice vectors, as they generally do not correspond to the lattice vectors of an unstrained quadrupole array.

To extract an estimate of the Peierls stress, we then follow a procedure analogous to that in Section 2, applying strain until the dislocations move. Here, rather than applying the strain to the fixed region ($R1 < r < R2$), we strain the *unrelaxed* lattice vectors. Then, we then compute the critical stress from the strain through the elastic constant matrix,

$$\sigma = \mathbf{C} \cdot \epsilon, \quad (1)$$

where σ is a column vector of the stresses, ϵ is the applied strain vector, and \mathbf{C} is the elastic constant matrix, *assumed* to equal that of the bulk material. The advantage of this approach is that it requires exploration of a minimal number of configurations and bulk lattice and elastic constants are relatively easy to obtain from first principles calculations. The disadvantage of this approach is that its underlying assumptions cast doubt of the accuracy of the results for unit cells of modest size.

Figure 5 explores the convergence of this approach with increasing cell size for calculation of the first Peierls stress ($P1$). The two smallest cells contain 90 atoms ($\sim 2.9\text{\AA} \times 24\text{\AA} \times 24\text{\AA}$) and 270 atoms ($\sim 2.9\text{\AA} \times 42\text{\AA} \times 42\text{\AA}$) (or 45 and 135 atoms, if symmetry is exploited), and are the only cells convenient for detailed *ab initio* studies. The results in these cells, however, are extremely poor, with errors of 200% and 53%, respectively. Thus, great care must be taken when working with such small cells and a method is needed to correct for these finite-size effects.

4 Corrections

The preceding calculations make two major assumptions: (1) that the quadrupole array of dislocations does not change the elastic constant matrix from that of bulk material, and (2) that the use of unrelaxed lattice vectors is appropriate. To explore the impact of these assumptions, we repeat the above calculations while using both the relaxed lattice vectors and elastic constants of the quadrupolar array.

Numerical calculations show that the symmetry of the elastic constant matrix of the quadrupolar array (\mathbf{C}') is the same as that of the bulk, although the individual components may differ. In particular, the stress-strain relation takes the form

$$\sigma = \mathbf{C}' \cdot \epsilon \quad (2)$$

$$\begin{bmatrix} \sigma_{xx} \\ \sigma_{yy} \\ \sigma_{zz} \\ \sigma_{yz} \\ \sigma_{xz} \\ \sigma_{xy} \end{bmatrix} = \begin{bmatrix} (4 \times 4) & 0 \\ 0 & (2 \times 2) \end{bmatrix} \cdot \begin{bmatrix} \epsilon_{xx} \\ \epsilon_{yy} \\ \epsilon_{zz} \\ \epsilon_{yz} \\ \epsilon_{xz} \\ \epsilon_{xy} \end{bmatrix} \quad (3)$$

In this equation, the lower 2×2 sub-block couples the σ_{xz} and σ_{xy} stresses only to the corresponding strains, while the upper 4×4 block couples the $\sigma_{xx}, \sigma_{yy}, \sigma_{zz}$ and σ_{yz} stresses only to their corresponding strains. Note, therefore, that for the present Peierls stress calculations only the lower 2×2 block is relevant.

Figure 6 shows the results (diamonds in the figure) of the extraction of the Peierls stress when using relaxed lattice vectors and the elastic constants for the quadrupole. The figure shows that the Peierls stress now converges much more quickly with cell size. (The figure does not include results for the smallest cell, which proved unstable to the relaxation of the lattice vectors.) For the smallest stable cell (135 atoms including symmetry), the error is reduced from 53% to only 18%, indicating the possibility of extracting reasonable results from cells of size suited to *ab initio* calculations. Although results for reasonably sized cells are accurate, this approach, however, is not necessarily well suited for *ab initio* calculations because relaxation of the lattice vectors and the calculation of the elastic constant matrix requires the exploration of many new atomic configurations.

5 Accurate and Efficient Peierls Stress Calculation

Having found an accurate approach, we now explore how to minimize that calculations associated with the above corrections. We begin by considering the necessity of relaxing the lattice vectors and then consider computation of the *relevant* components of the elastic constant matrix \mathbf{C}' .

5.1 Benefit of fixed lattice vectors

Working with unrelaxed lattice vectors generates spurious strains in the unit cell. The question is whether these strains create spurious stresses which confound the extraction of the Peierls stress. The elastic force which any such stresses would generate on the dislocation take the form [16]:

$$\mathbf{F}_L = \mathbf{b} \cdot \boldsymbol{\sigma} \times \boldsymbol{\eta}. \quad (4)$$

Here, \mathbf{F}_L is the force per unit length on the dislocation, \mathbf{b} is the Burgers vector, $\boldsymbol{\sigma}$ is the stress tensor written as a *matrix*, and $\boldsymbol{\eta}$ is the sense vector, the direction along which the dislocation runs. For a [111]-screw dislocation \mathbf{b} and $\boldsymbol{\eta}$ both lie along the z -axis, and, therefore, only two components of stress can generate a force on the dislocation, σ_{xz} and σ_{yz} , and confound the extraction of the Peierls stress. We now consider whether the strains associated with the unrelaxed lattice vectors can generate such stresses. We distinguish two types of strain, dilation and shear.

The presence of the quadrupolar array tends to dilate the unit cell in the (111) plane. Due to symmetry, this dilation tends to be uniform, as we have confirmed by direct numerical calculation on the unit cells. The above form of the elastic constant matrix \mathbf{C}' prevents such dilation from generating any σ_{xz} component. The second confounding component σ_{yz} would also vanish were the 4×4 subblock of the elastic constant matrix to have precisely the same symmetry as that of the bulk. Numerically, we find that that this is almost the case, and that the dilation contribution

to σ_{yz} ranges from 0.02% (in our largest cell) to only 4% (in the 135 atom cell) of the stress experienced in the *unrelaxed* cell. The diagonal components of strain ϵ_{ii} do not significantly affect the extraction of the Peierls stress, and therefore need not be relaxed to extract meaningful Peierls stresses.

Turning to shear strains, the equal spacing of the dislocation array leads to zero shear within linear elasticity theory. From symmetry, however, core-core interaction (non-elastic) can generate a force in the $[1\bar{1}0]$ -direction only, Figure 7, which results in one non-zero component of strain, ϵ_{yz} . From direct calculations it is shown that this is in fact the only non-zero component of shear strain. Relaxing this component of strain, therefore, creates a artificial material environment, different from what isolated dislocations would experience. To more quickly approach the limit of isolated dislocations, one should therefore *not* relax this component of the strain. This advantage of using of unrelaxed lattice vectors is well known and commonly exploited in the materials literature in the study of *two*-dimensional defects such as grain boundaries or surfaces[18, 19]. We therefore expect to be able to extract accurate Peierls stresses without the need for relaxing either off-diagonal or diagonal components of strain.

Figure 6 shows the results (circles in the figure) of extracting the Peierls stress when using *unrelaxed* lattice vectors, but while still computing the stresses with the appropriate elastic constant matrix \mathbf{C}' . The results converge even more quickly than those obtained by relaxing the lattice vectors, thus supporting our analysis. Therefore, extremely good results (already within 2% in the 135 atom cell) can be obtained by not relaxing the lattice vectors. This not only produces results of far superior quality, it also reduces the computational effort.

5.2 Extraction of elastic constants

The results of Section 5.1, while quite impressive, still require calculation of the elastic constant matrix \mathbf{C}' of the quadrupolar array. Significant savings can be gained with the simple realization that only the 2×2 sub-block of the elastic constant matrix enters calculation of $P1$ and $P2$ through Eq. 3. Moreover, within linear elasticity theory, these components can be extracted equally well at the relaxed or unrelaxed lattice vectors, thereby again mitigating the need for relaxation of the lattice vectors.

Not all of the components of the 2×2 sub-block,

$$\mathbf{C}'_2 \equiv \begin{bmatrix} C'_{44} & -C'_{16} \\ -C'_{16} & C'_{55} \end{bmatrix}, \quad (5)$$

need be computed independently.

To see this, consider the application of a pure, shear strain ϵ_{xz} to the system. As a result of the symmetry of \mathbf{C}' , this generates only two components of stress, σ_{xz} and σ_{xy} . From equation 4, however, σ_{xy} does not generate any forces on the dislocation and thus, within linear elasticity, does not effect our calculation of the Peierls stress. The remaining stress, whose critical value is the Peierls stress, can be computed from just one component of \mathbf{C}'_2 ,

$$\sigma_{xz} = C'_{44}\epsilon_{xz}. \quad (6)$$

Finally, we note that this pre-factor can be extracted without any additional calculation. Figure 8 shows the total energy of the quadrupole array plotted as a function of strain during the extraction of the critical Peierls stress. Prior to the first dislocation glide event at $\epsilon_{xz} \approx 0.015$, the energy increases quadratically according to

$$\Delta E = \frac{1}{2}C'_{44}\epsilon_{xz}^2, \quad (7)$$

which contains precisely the same pre-factor as in Eq. 6.

Figure 6 shows the result (triangles in the figure) of the extraction of the Peierls stress from the application of a pure, shear strain ϵ_{xz} to the *unrelaxed* lattice vectors and extracting the relevant elastic constant from the curvature of the energy prior to the glide events. The results are of nearly the same quality as working with unrelaxed lattice vectors and using the full elastic constant matrix \mathbf{C}' .

5.3 Second Peierls stress: $P2$

Figure 9 shows our preliminary results for the extraction of the second Peierls stress $P2$. These results are complicated by the fact that after the first transition $P1$, the quadrupole array is now distorted and no longer a perfect quadrupole, thereby generating non-negligible dislocation-dislocation forces and further modifying the elastic constant matrix of the cell. As a possible correction to this effect, we are presently exploring moving the distorted cores back to their original quadrupole locations before further increasing the stress. Nonetheless, we find that significant improvements can be made by using the elastic constant matrix of a perfect quadrupole array and ignoring the dislocation-dislocation interactions. Finally, results for pure shear calculations are quite encouraging.

6 Conclusion

This paper presents an accurate and effective way to calculate the $\{110\}$ Peierls stress in a $[111]$ screw dislocation in a bcc material. The results show that accurate results can be obtained even for the smallest cells while using unrelaxed lattice vectors and extracting the elastic constants directly from the calculations. The method most importantly appears to make *ab initio* calculations of Peierls stresses viable in periodic boundary conditions for the first time.

References

- [1] G. Wang, A. Strachan, T. Cagin, and W.A. GoddardIII. *Mater. Sci. and Engng.*, 2001.
- [2] V. J. Shenoy and R. Phillips. *Phil. Mag. A*, 76:367, 1997.
- [3] J. A. Moriarty, W. Xu, P. Söderlind, L. H. Yang, and J. Zhu. *J. Engng. Mater. Technol.*, 121:120, 1999.
- [4] W. Xu and J. A. Moriarty. *Comp. Mater. Sci.*, 9:348, 1998.
- [5] S. Takeuchi. Core structure and glide behavior of a screw dislocation in the bcc lattice. In J. K. Lee, editor, *Interatomic Potentials and Crystalline Defects*, page 201, 1980.
- [6] L. H. Yang, Söderlind P., and J. A. Moriarty. *Phil. Mag. A* future issue.
- [7] V. V. Bulatov, O. Richmond, and M. V. Glasov. *Acta Mater.*, 47:3507, 1999.
- [8] S. Rao and C. Woodward. *Phil. Mag. A* future issue.
- [9] S. Rao, C. Hernandez, J. Simmons, T. Parthasarathy, and C. Woodward. *Phil. Mag. A*, 77:231, 1998.

- [10] Marklund S. *Phys. Status Solidi B*, 85:673, 1978.
- [11] J. R. K. Bigger and *et. al.* *Phys. Rev. Lett.*, 69:2224, 1992.
- [12] N. Lehto and S. Oberg. *Phys. Rev. Lett.*, 80:5568, 1998.
- [13] A. Strachan, T. Cagin, O. Gulseren, S. Mukherjee, R. E. Cohen, and W. A. Goddard III. *In preperation.*
- [14] A. N. Stroh. *Phil. Mag.*, 3:625, 1958.
- [15] A. K. Head. *Phys. Stat. Sol.*, 6:461, 1964.
- [16] J. P. Hirth and J. Lothe. *Theory of Dislocations*. John Wiley and Sons, 2 edition, 1982.
- [17] V. Vitek. *Cryst. Lattice Defects*, 5:1, 1974.
- [18] T.A. Arias and J.D. Joannopoulos. *Phys. Rev. Lett.*, 69:3330, 1992.
- [19] J. Wang, T.A. Arias, and J.D. Joannopoulos. *Phys. Rev. B*, 47:10497, 1993.

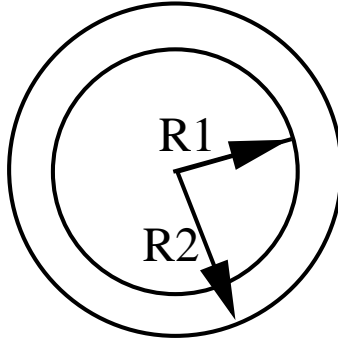


Figure 1: Peierls stress calculation within cylindrical boundary conditions: atoms whose distance from the center is less than $R1$ are relaxed under inter-atomic potential forces, while those in the region between $R1$ and $R2$ are held fixed to the anisotropic elasticity theory solution.

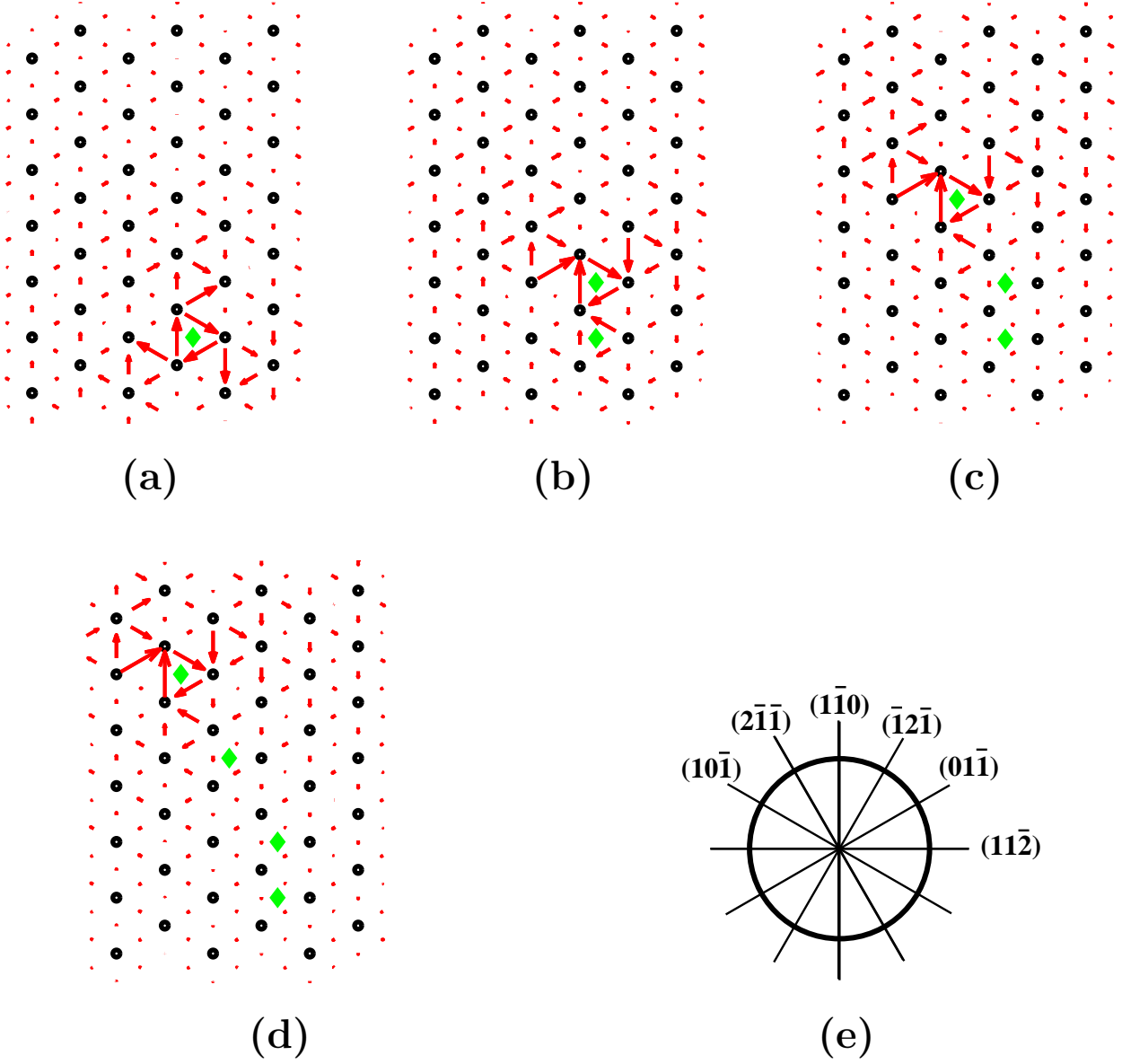


Figure 2: Differential displacement (DD) maps of a $[111]$ screw dislocation at increasing stress computed within cylindrical boundary conditions: **a)** zero applied stress, **b)** initial jump along $(1\bar{1}0)$ at a stress ≥ 0.74 GPa ($P1$), **c)** second jump, along $(2\bar{1}\bar{1})$ at a stress ≥ 0.91 GPa ($P2$), **d)** subsequent jump along $(2\bar{1}\bar{1})$, **e)** orientation of $\{110\}$ and $\{112\}$ planes.

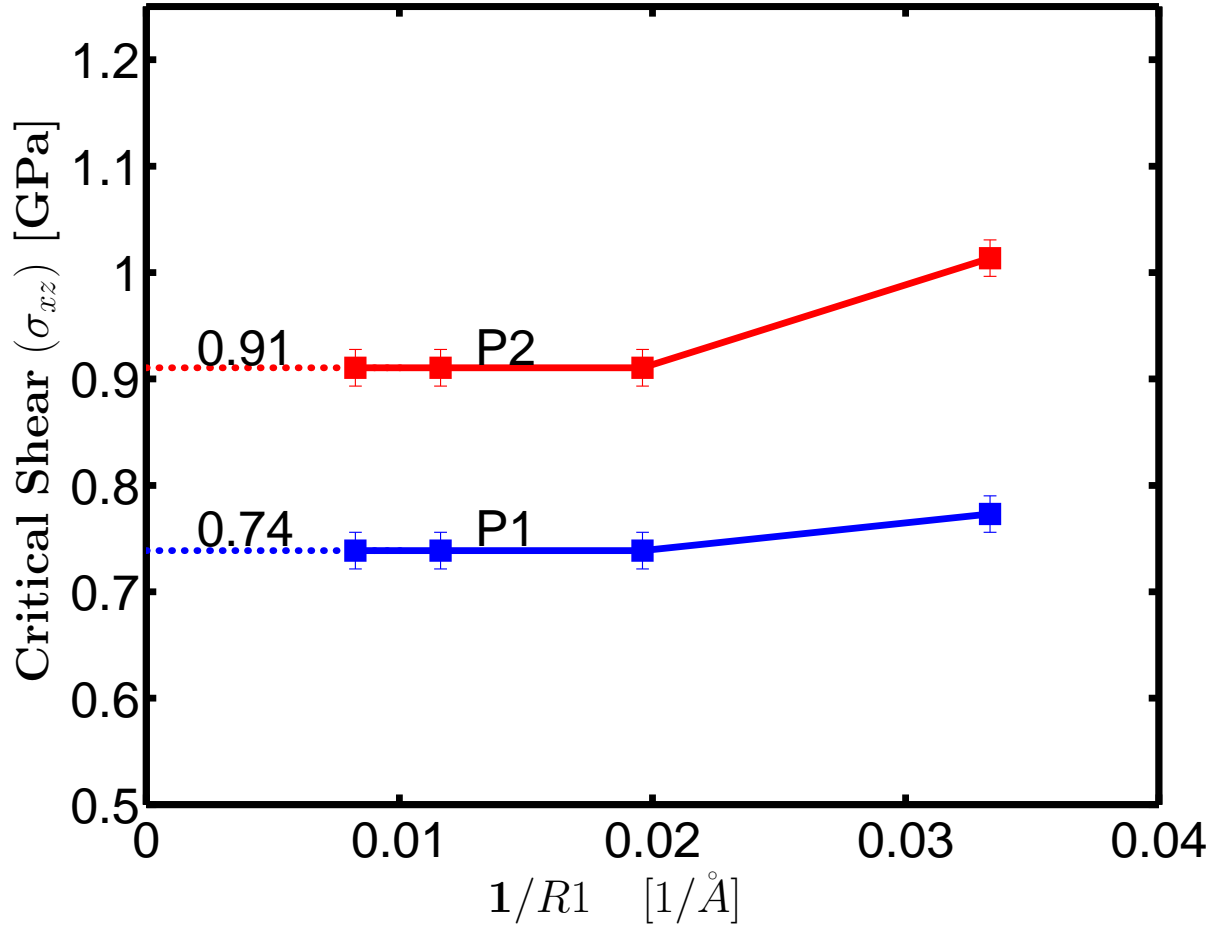


Figure 3: Convergence of P1 and P2 as a function of $1/R1$, for cylinders ranging from $R1 = 30\text{\AA}$ to $R1 = 120\text{\AA}$.

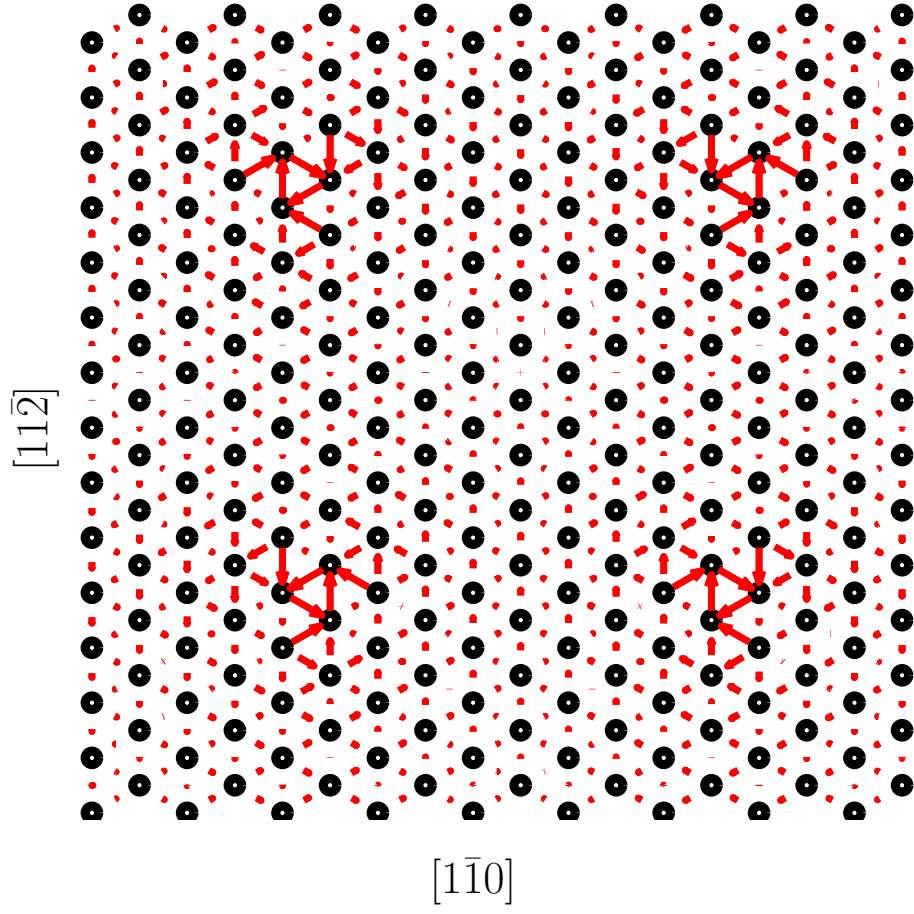


Figure 4: Dislocation displacement (DD) map of a quadrupole dislocation array within a 270 atom cell with periodic boundary conditions. The cell may be reduced to 135 atoms with appropriate choice of lattice vectors.

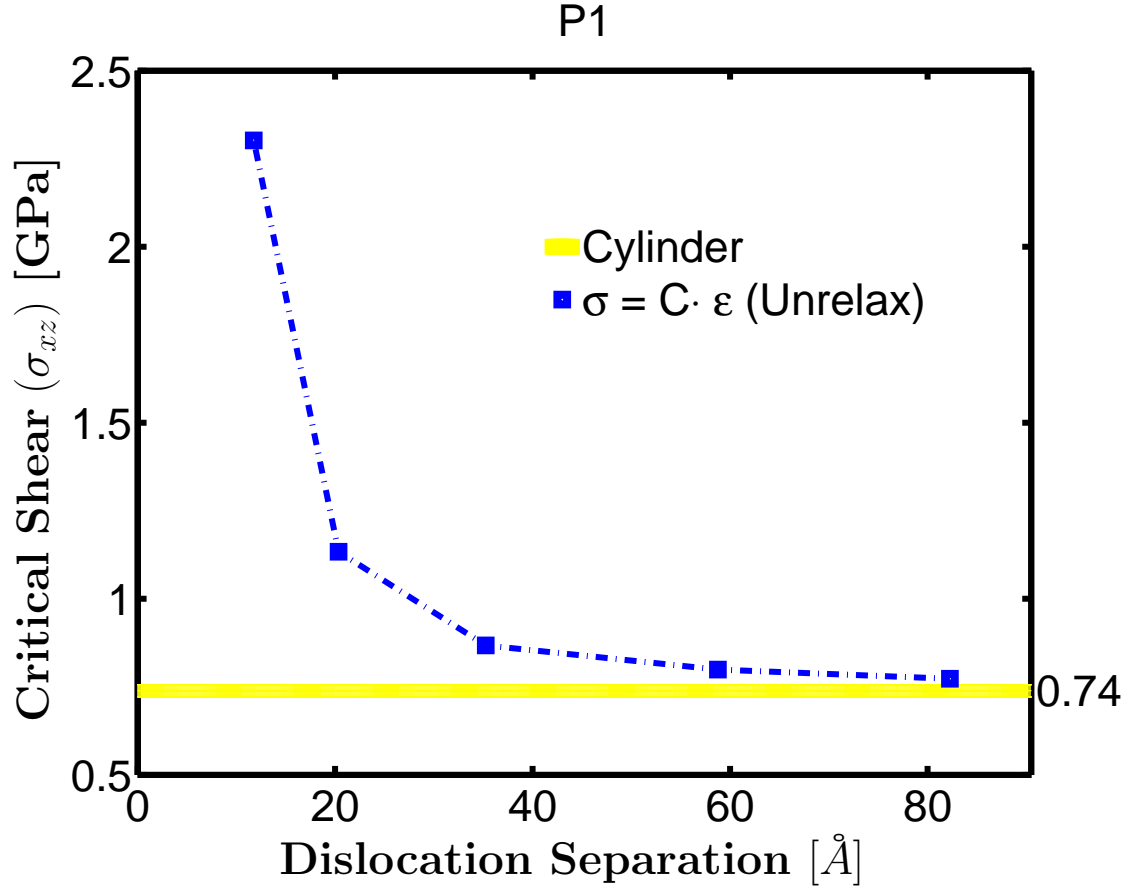


Figure 5: Convergence of P1 calculated within periodic boundary conditions using unrelaxed lattice vectors and bulk elastic constants: Peierls stress calculated using Eq. 1 (squares), limit exacted from Figure 3 (solid line with width indicating numerical uncertainty). Uncertainties in the periodic calculations are smaller than the square symbols.

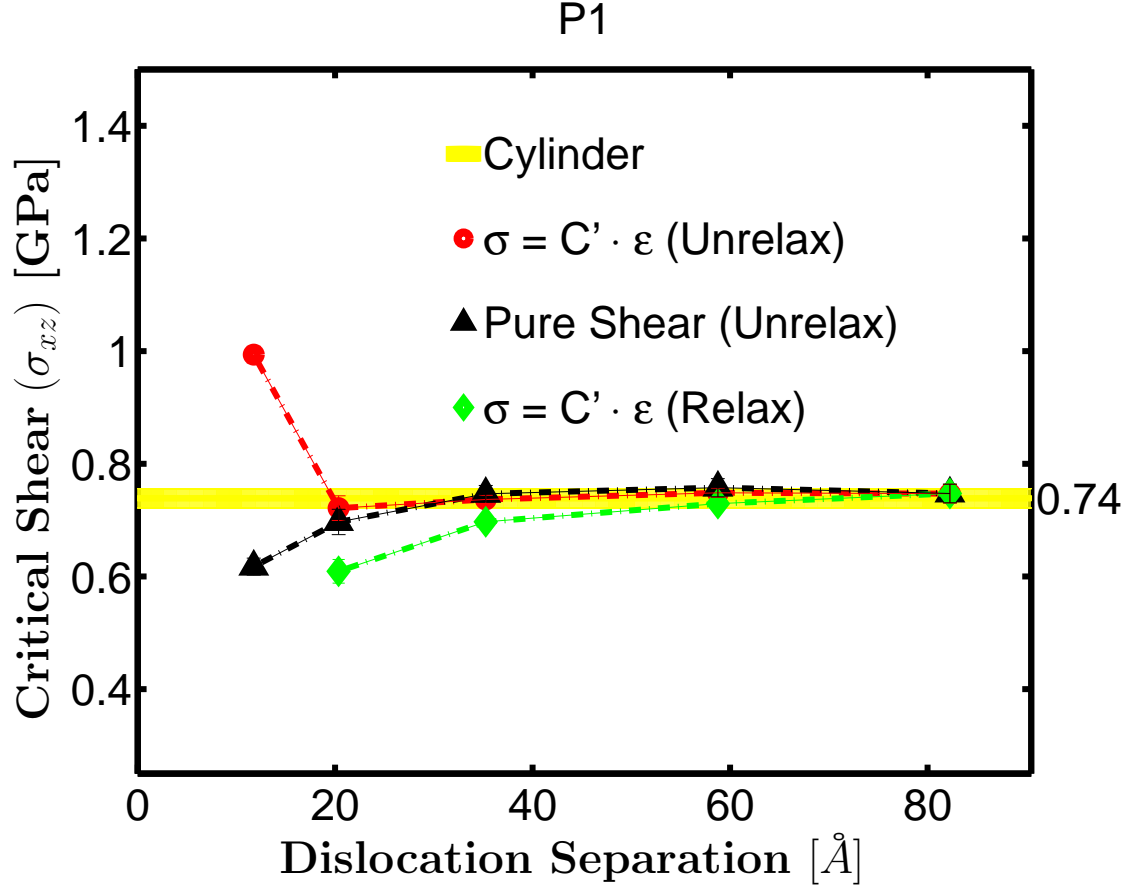


Figure 6: Convergence of P1 calculated within periodic boundary conditions: using relaxed lattice vectors and quadrupolar elastic constants (diamonds), using unrelaxed lattice vectors and quadrupolar elastic constants (circles), using unrelaxed lattice vectors, pure shear and elastic constants extracted during the calculation (triangles), asymptotic result extracted from cylindrical boundary conditions (horizontal line). Error bars associated with quadrupolar array are generally smaller than the associated icons.

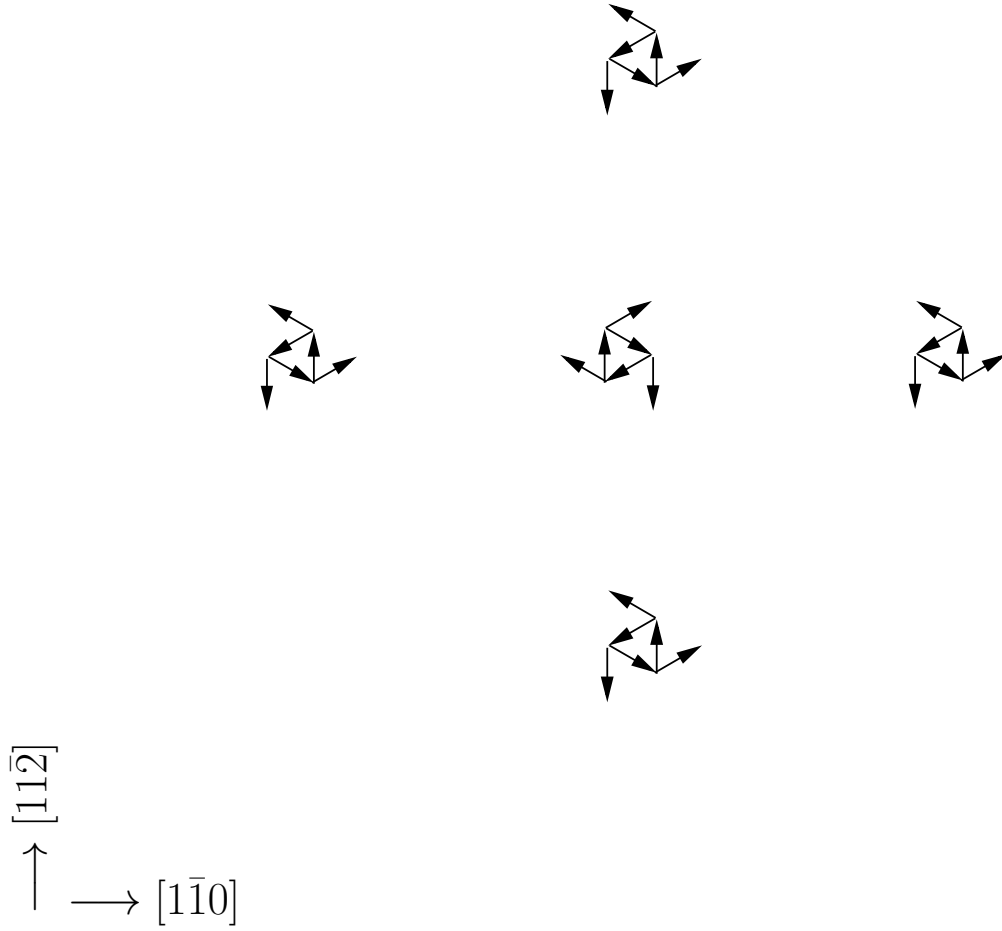


Figure 7: The first nearest neighbors cannot generate any elastic force on the center dislocation, since they are equally spaced. From the core asymmetry there can be a core-core force in only in the $[1\bar{1}0]$. Note that these symmetry arguments works for higher order neighbors too.

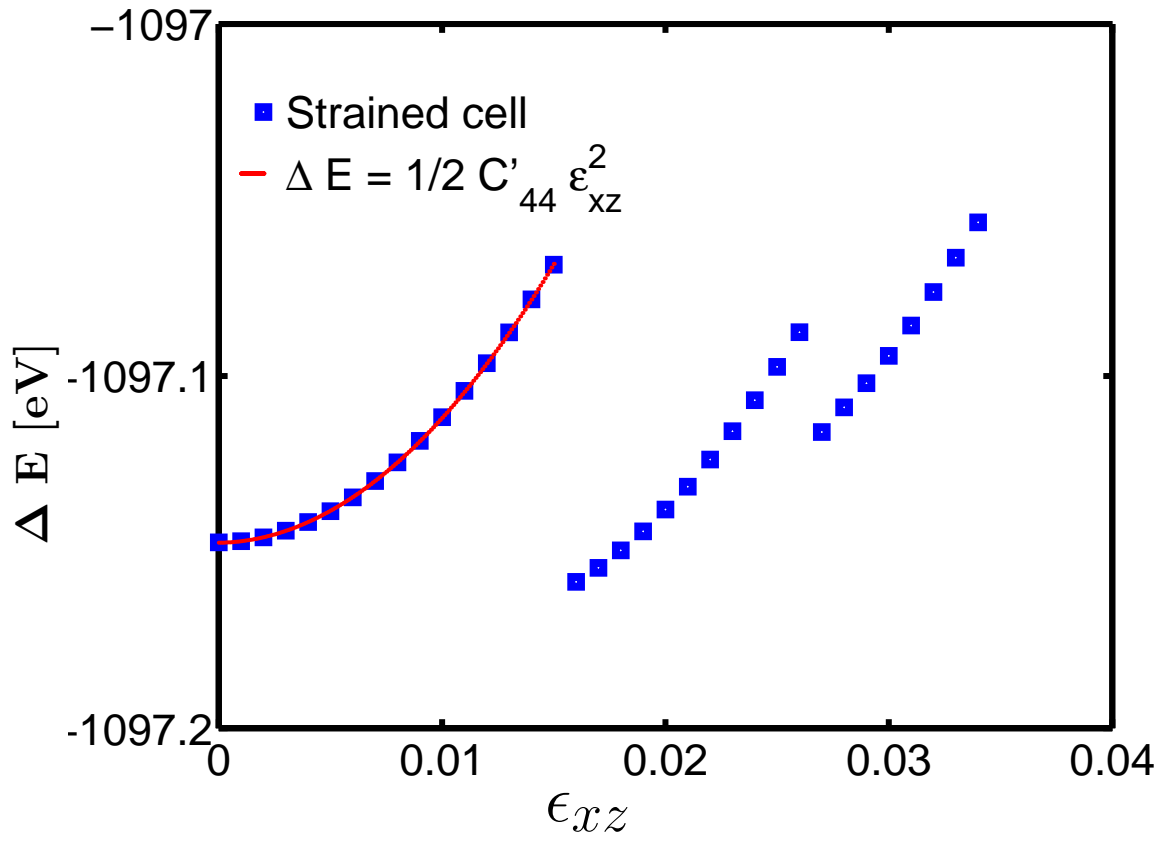


Figure 8: Energy of a $42\text{\AA} \times 42\text{\AA} \times 2.9\text{\AA}$ cell (270 atoms) plotted as a function of applied pure shear strain ϵ_{xz} : direct calculations (squares), quadratic fit (curve).

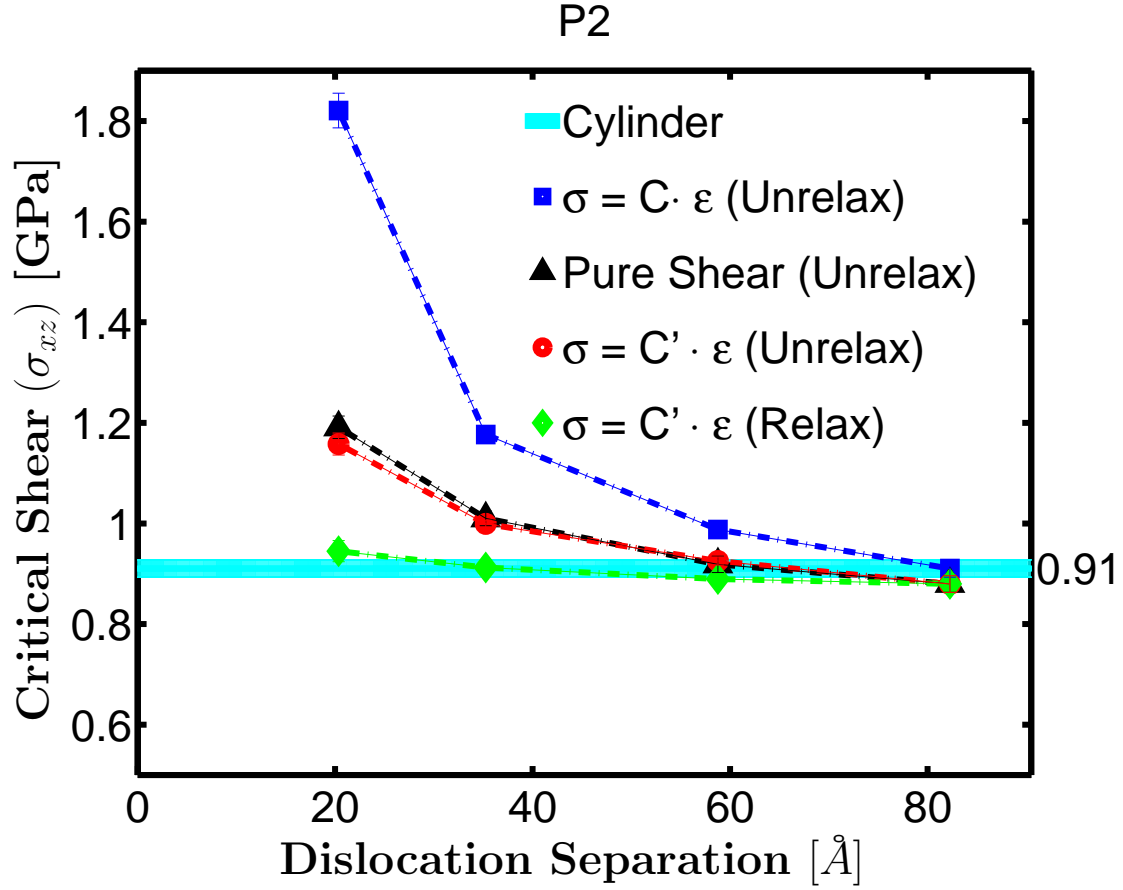


Figure 9: Convergence of P2 calculated within periodic boundary conditions: using unrelaxed lattice vectors and bulk elastic constants (squares), using relaxed lattice vectors and quadrupolar elastic constants (diamonds), using unrelaxed lattice vectors and quadrupolar elastic constants (circles), using unrelaxed lattice vectors, pure shear and elastic constants extracted during the calculation (triangles), asymptotic result extracted from cylindrical boundary conditions (horizontal line).